Performance analysis of air cooled block type aluminum foam heat sinks of different pore densities

*[1]İsmail Solmuş and [2]Cihan Yıldırım
*[1] Department of Mechanical Engineering, Atatürk University, 25240 Erzurum, Turkey
[2] Department of Mechanical Engineering, Adana Science and Technology University, 01180 Adana, Turkey

Abstract

This study numerically investigates the thermal and fluid flow performances of air cooled block type aluminum foam heat sinks of different pore densities inserted in a rectangular channel. The upper wall of the channel is thermally insulated while the lower wall is maintained at a constant temperature. A two energy equation model with the Brinkman-Forchheimer extended Darcy model is employed. The governing conservation equations are simultaneously solved with the finite volume technique. Numerical simulations are performed with air-cooled open cell aluminum foams of different pore densities such as 10, 20 and 40 PP. The local and average Nusselt numbers at the constant temperature wall and pressure drop along the flow direction for each sample are presented for a wide range of Reynolds number (*Re*) =500-9500. It is found that thermal performance of heat sink material investigated is almost independent of the amount of pores per inch. Conversely, its effect on the fluid flow performance of that is significant.

Key words: Porous media, Aluminum foam, Heat removal, Pressure drop,

Nomenclature

C_p	specific heat at constant pressure (J/kg°C)
C_F	inertial coefficient
Da	Darcy number $[K/H^2]$
d_p	pore diameter (m)
d_f	fiber diameter (m)
H	height of the porous insert (m)
h_v	heat transfer coefficient between solid and fluid phases (W/m^2K)
K	permeability (m^2)
k	thermal conductivity (W/mK)
L	length of the porous insert (m)
$\overline{Nu}$	average Nusselt number
Nu	local Nusselt number
Nu_{fs}	fluid-to-solid Nusselt number $[h_v\alpha_{sf}H^2/k_f]$
P	dimensionless pressure $[p/\rho_f u_i^2]$
Pr	Prandtl number (v/α)
p	pressure (Pa)
Re	Reynolds number $[\rho_f u_i H/\mu]$

*Corresponding author: Address: Department of Mechanical Engineering, Atatürk University, 25240 Erzurum, Turkey. E-mail address: er24dem@gmail.com, Phone: +904422314845 Fax: +904422360957

Re_d	Reynolds number based on the pore diameter $[\rho_f u_i d_p/\mu]$
T	temperature (°C)
U	dimensionless velocity in the x-direction $[u/u_i]$
U_M	dimensionless magnitude of the velocity $[\sqrt{u^2+v^2}/u_i]$
u	velocity component in the x-direction (m/s)
V	dimensionless velocity in the y-direction $[v/u_i]$
v	velocity component in the y-direction (m/s)
X, Y	dimensionless Cartesian coordinates
x, y	Cartesian coordinates (m)

Greek symbols

ε	Porosity
ρ	Density (kg/m^3)
μ	dynamic viscosity (kg/ms)
θ	dimensionless temperature $[(T-T_i)/(T_w-T_i)]$
α_{sf}	specific surface area (m^{-1})

Subscripts

d	thermal dispersion
f	fluid
fe	fluid effective
i	inlet
s	solid
se	solid effective
w	wall

1. Introduction

The overheating in electronic components still is a major concern for the producers. Conventional cooling methods such as air-cooled metal finned heat sinks are not adequate for removing dissipated heat from such components. The open cell metal foam heat sinks seem an attractive solution to overcome overheating in electronic components due to their high surface area to volume ratio and strong flow mixing capabilities. Several experimental and numerical studies on the open-cell metal foams have been conducted in the recent years. Li et al., [1] numerically studied the fluid flow and heat transfer characteristics of staggered porous blocks in a channel. Solmuş [2] conducted a numerical study to investigate the thermal and fluid flow performances of the block type graphite and aluminum foam heat sinks in a rectangular channel. Yang and Hwang [3] numerically examined the turbulent heat transfer enhancement in the pipe filled with porous media. Dukhan and Chen [4] provided experimental data of heat transfer inside

*Corresponding author: Address: Department of Mechanical Engineering, Atatürk University, 25240 Erzurum, Turkey. E-mail address: er24dem@gmail.com, Phone: +904422314845 Fax: +904422360957

rectangular blocks of open-cell aluminum foam. Leong and Jin [5] performed an experimental study to investigate the heat transfer performance of aluminum foam heat sinks of different pore densities subjected to oscillating flow. Feng et al. [6] conducted a combined experimental and numerical study on finned and unfinned aluminum foam heat sinks under impinging air jet cooling for different foam heights and Reynolds number.

In this study, thermal and fluid flow performances of air cooled block type aluminum foam heat sinks of different pore densities inserted in a rectangular channel are investigated numerically over a wide range of *Re* =500-9500.

2. Problem Description

Fig. 1 depicts the computational domain considered in this study. A block of open-cell aluminum foam is inserted in a rectangular channel. The upper wall of the channel is thermally insulated while the lower wall is maintained at a constant temperature. Air enters the channel with a uniform velocity and temperature and flows through the block of foam. The height and length of the heat sink are fixed as 25 and 50 mm, respectively.

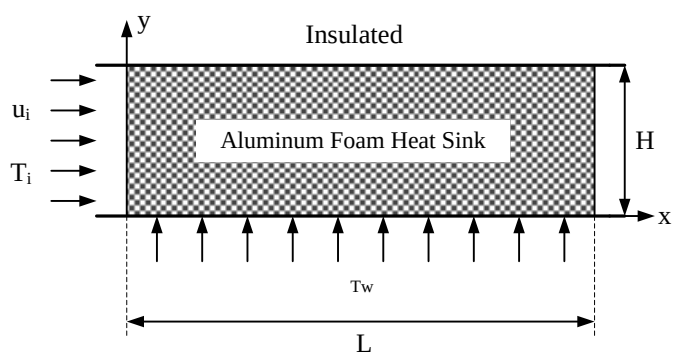

Figure 1. Computational domain.

3. Mathematical Formulation

The local volume averaging method has been used to drive the governing macroscopic conservation equations from the microscopic ones. The mathematical model with the boundary conditions proposed in this study is primarily based on the following assumptions and simplifications:

- the foam porosity is spatially uniform and constant
- the flow is steady, laminar and incompressible
- heat transfer by radiation and natural convection, viscous dissipation and the work done by pressure changes are neglected
- thermo-physical properties of the solid and fluid phases are assumed to be constant
- there is no gap between the block of foam and channel walls

- the thickness of the top and bottom channel walls are assumed to be very thin and hence, their thermal resistances are neglected
- thermal contact resistances at the interfaces are not considered.
- side walls of the channel are assumed to be well insulated and thus, the two dimensional approach is used.
- the local non-thermal equilibrium between the solid and fluid phases is considered.

3.1. *Governing equations*

Under the assumptions and simplifications above, the two dimensional steady state macroscopic conservation equations for mass, momentum and energy of solid and fluid phases are as follows;

Continuity equation:

$$\frac{\partial u}{\partial x}+\frac{\partial v}{\partial y}=0 \tag{1}$$

Momentum equations:

The Brinkman-Forchheimer extended Darcy model valid for both Darcy and non-Darcy regimes was used to obtain the velocity distribution inside porous material and given as follows;

x-momentum equation:

$$\frac{\rho_f}{\varepsilon^2}\left(u\frac{\partial u}{\partial x}+v\frac{\partial u}{\partial y}\right)=-\frac{\partial p}{\partial x}-\frac{\mu u}{K}-\frac{\rho_f C_F}{\sqrt{K}}|\vec{V}|u+\frac{\mu}{\varepsilon}\left(\frac{\partial^2 u}{\partial x^2}+\frac{\partial^2 u}{\partial y^2}\right) \tag{2}$$

y-momentum equation:

$$\frac{\rho_f}{\varepsilon^2}\left(u\frac{\partial v}{\partial x}+v\frac{\partial v}{\partial y}\right)=-\frac{\partial p}{\partial y}-\frac{\mu v}{K}-\frac{\rho_f C_F}{\sqrt{K}}|\vec{V}|v+\frac{\mu}{\varepsilon}\left(\frac{\partial^2 v}{\partial x^2}+\frac{\partial^2 v}{\partial y^2}\right) \tag{3}$$

- Energy conservation equations:

The local thermal non equilibrium (LTNE) between the phases is in existence and thus, the two different energy conservation equations are proposed.

Energy conservation equation for the fluid phase:

$$(\rho C_p)_f\left(u\frac{\partial T_f}{\partial x}+v\frac{\partial T_f}{\partial y}\right)=h_v\,a_{sf}(T_s-T_f)+(k_{fe}+k_d)\frac{\partial^2 T_f}{\partial x^2}+(k_{fe}+k_d)\frac{\partial^2 T_f}{\partial y^2} \tag{4}$$

Energy conservation equation for the solid phase:

$$0 = h_v\, a_{sf}\left(T_f - T_s\right) + k_{se}\frac{\partial^2 T_s}{\partial x^2} + k_{se}\frac{\partial^2 T_s}{\partial y^2} \tag{5}$$

The equations above are non-dimensionalized by introducing the following dimensionless parameters:

$$X = \frac{x}{H} \quad Y = \frac{y}{H} \quad U = \frac{u}{u_i} \quad V = \frac{v}{u_i} \quad P = \frac{p}{\rho_f u_i^2} \quad Da = \frac{K}{H^2}$$

$$Re = \frac{\rho_f u_i H}{\mu} \quad U_M = \frac{\sqrt{u^2 + v^2}}{u_i} \quad Nu_{fs} = \frac{h_v \alpha_{sf} H^2}{k_f} \quad \theta = \frac{T - T_i}{T_w - T_i}$$

Non-dimensional continuity equation:

$$\frac{\partial U}{\partial X} + \frac{\partial V}{\partial Y} = 0 \tag{6}$$

- Non-dimensional momentum equations:

Non-dimensional x-momentum equation:

$$\left(U\frac{\partial U}{\partial X} + V\frac{\partial U}{\partial Y}\right) = -\varepsilon^2\frac{\partial P}{\partial X} - \frac{\varepsilon^2}{ReDa}U - \frac{\varepsilon^2 C_F U_M}{\sqrt{Da}}U + \frac{\varepsilon}{Re}\left(\frac{\partial^2 U}{\partial X^2} + \frac{\partial^2 U}{\partial Y^2}\right) \tag{7}$$

Non-dimensional y-momentum equation:

$$\left(U\frac{\partial V}{\partial X} + V\frac{\partial V}{\partial Y}\right) = -\varepsilon^2\frac{\partial P}{\partial Y} - \frac{\varepsilon^2}{ReDa}V - \frac{\varepsilon^2 C_F U_M}{\sqrt{Da}}V + \frac{\varepsilon}{Re}\left(\frac{\partial^2 V}{\partial X^2} + \frac{\partial^2 V}{\partial Y^2}\right) \tag{8}$$

- Non-dimensional energy conservation equations:

Non-dimensional energy conservation equation for the fluid phase:

$$U\frac{\partial \theta_f}{\partial X} + V\frac{\partial \theta_f}{\partial Y} = \frac{Nu_{fs}}{RePr}\left(\theta_s - \theta_f\right) + \frac{1}{RePr}\left(\frac{k_{fe} + k_d}{k_f}\right)\left(\frac{\partial^2 \theta_f}{\partial X^2} + \frac{\partial^2 \theta_f}{\partial Y^2}\right) \tag{9}$$

Non-dimensional energy conservation equation for the solid phase:

$$0 = Nu_{fs}(\theta_f - \theta_s) + \frac{k_{se}}{k_f}\left(\frac{\partial^2 \theta_s}{\partial X^2} + \frac{\partial^2 \theta_s}{\partial Y^2}\right) \tag{10}$$

The thermal dispersion conductivity is given by [7] as follow;

$$k_d = 0.025\left(\rho c_p\right)_f \sqrt{K} u_i \tag{11}$$

The effective thermal conductivities are evaluated by the following formulas proposed by Calmidi and Mahajan [8]:

$$k_{fe} = \varepsilon k_f \tag{12}$$

$$k_{se} = 0.181(1-\varepsilon)^{0.763} k_s \tag{13}$$

The interior surface area to volume ratio of the aluminum foam is calculated by [9]:

$$\alpha_{sf} = \frac{3\pi d_f\left(1 - e^{-((1-\varepsilon)/0.04)}\right)}{\left(0.59 d_p\right)^2} \tag{14}$$

where,

$$\frac{d_f}{d_p} = 1.18\sqrt{\frac{1-\varepsilon}{3\pi}}\left(\frac{1}{1 - e^{-((1-\varepsilon)/0.04)}}\right) \tag{15}$$

The local and average Nusselt numbers are defined, respectively as follows:

$$Nu = \frac{hH}{k_f} = -\frac{k_{se}}{k_f}\left(\frac{\partial \theta_s}{\partial Y}\right)_{Y=0} - \frac{k_{fe}}{k_f}\left(\frac{\partial \theta_f}{\partial Y}\right)_{Y=0} \tag{16}$$

$$\overline{Nu} = \frac{\bar{h}H}{k_f} = \frac{H}{L}\int_0^{L/H} Nu dX \tag{17}$$

The thermo-physical properties of aluminum foam heat sinks of different pore densities are presented in Table 1.

Table 1. Thermo-physical properties of aluminum foams considered herein [10].

	ε	PPI	d_f (mm)	K (m^2)	C_F	Nu_{fs}
A	0.93	10	0.4	7.838*10^{-8}	0.019	$0.0077Re_d^{1.277}$
B	0.93	20	0.21	5.308*10^{-8}	0.02	$0.00249Re_d^{1.277}$
C	0.93	40	0.11	2.717*10^{-8}	0.02	$0.00622Re_d^{1.277}$

3.2. *Boundary conditions*

The boundary conditions and their dimensionless forms for the solution of the governing conservation equations are presented in Table 2 and Table 3, respectively.

4. Numerical Procedure

The governing partial differential equations under consideration were solved numerically using the finite volume technique developed by Patankar [11]. A staggered uniform grid arrangement was employed. Scalar variables and velocities were defined at cell center and cell faces, respectively. The power-law was used to treat the combined convection–diffusion effect. Pressure velocity coupling was handled by the SIMPLER algorithm. The nonlinear algebraic equations were solved iteratively by the combination of the line by line method, and a block tridiagonal matrix solver algorithm (Thomas algorithm). In the simulation program, iterations were terminated when the following condition was satisfied by the variable ϕ:

$$R_{\emptyset,P} = \frac{|a_P \emptyset_P - \sum_{nb} a_{nb} \emptyset_{nb} - b|}{|a_P \emptyset_P|} < 10^{-6} \tag{18}$$

Where, ϕ and nb represent any dependent variables and cell neighbors of cell P, respectively.

Grid independence test is carried out to ensure the reliability of the numerical results. It is found that the grid size of 60*80 is sufficiently enough for the numerical accuracy.

Table 2. Boundary conditions

	u	v	T_f	T_s	$\frac{\partial u}{\partial x}$	$\frac{\partial v}{\partial x}$	$\frac{\partial T_f}{\partial x}$	$\frac{\partial T_s}{\partial x}$	$\frac{\partial T_f}{\partial y}$	$\frac{\partial T_s}{\partial y}$
$x = 0$	u_i	0	T_i					0		
$x = L$					0	0	0	0		
$y = 0$	0	0	T_w	T_w						
$y = H$	0	0							0	0

Table 3. Dimensionless form of the boundary conditions

	U	V	θ_f	θ_s	$\frac{\partial U}{\partial X}$	$\frac{\partial V}{\partial X}$	$\frac{\partial \theta_f}{\partial X}$	$\frac{\partial \theta_s}{\partial X}$	$\frac{\partial \theta_f}{\partial Y}$	$\frac{\partial \theta_s}{\partial Y}$
$X = 0$	1	0	0					0		
$X = L/H$					0	0	0	0		
$Y = 0$	0	0	1	1						
$Y = 1$	0	0							0	0

5. Results and discussion

The research investigates the heat and fluid flow characteristics of air-cooled open cell aluminum foams of different pore densities such as 10, 20 and 40 PP. The local and average Nusselt numbers at the constant temperature wall and pressure drop for each sample are presented over a range of Reynolds numbers (*Re)* =500-9500. Fig. 2a depicts the non-dimensional velocity profile inside the 10 PPI aluminum foam heat sink. It is found from the parametric study that the plug flow assumption is valid for each sample over a range of parameters interested. The same finding is reported by Yang and Hwang [12]. The variation of pressure drop along the flow direction with *Re* number for 10, 20 and 40 samples is presented in Fig.2b. It is obvious that an increase in *Re* number results in an increase in pressure drop and this finding is valid for each sample. The 40 PPI aluminum foam shows the highest resistance to the fluid flow along the flow direction due to its extremely low permeability value.

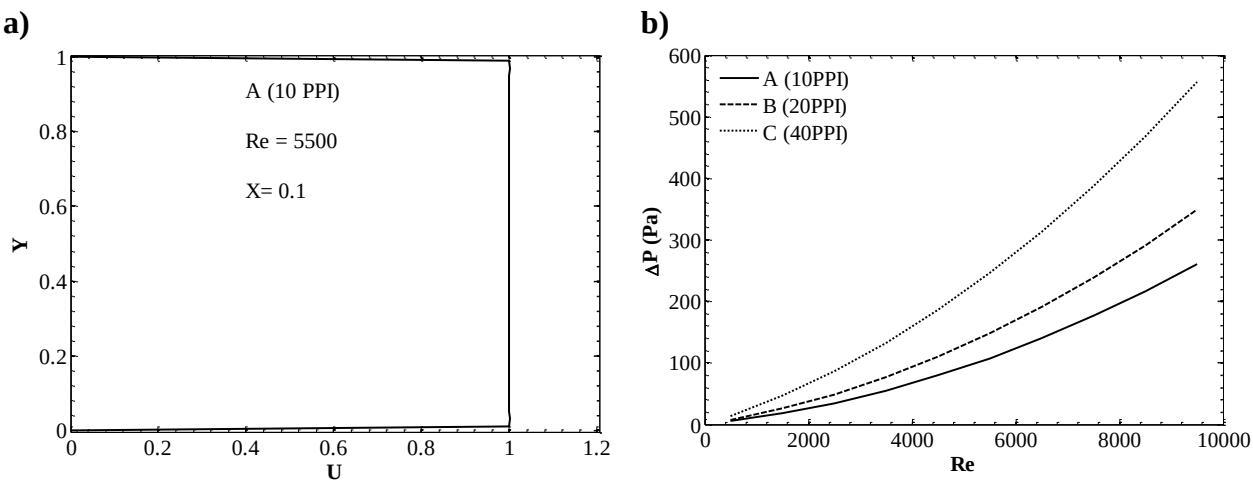

Figure 2. a) The dimensionless velocity profile inside the10 PPI aluminum foam, b) Variation of pressure drop with *Re* number for 10, 20 and 40 PPI aluminum foams

The variation of local Nusselt number (*Nu*) along the flow direction at the constant temperature wall is presented in Figs. 3a-c for 10, 20 and 40 PPI aluminum foams, respectively. Nusselt number at the channel entrance for all samples is comparatively high according to that along the rest of channel. Then, it shows a sharp decrease when *x/H* is nearly less than <0.25 and after that, it doesn't exhibit any significant variation until at the channel exit. It is clear that the local Nusselt number for each sample increases as Re number is increased. Local Nusselt number shows almost no dependence on the amount of pores per inch.

Fig.3d illustrates the variation of average Nusselt number with Reynolds number for 10, 20 and 40 PPI aluminum foams. It is obvious in Fig.3d that an increase in Reynolds number leads to an enhancement on the total heat removal performance of each sample. This due to fact that the amount of heat transfer from the constant temperature wall by convection increases as the Reynolds number is increased. However, a special attention needs to be given that increasing

Reynolds number has a negative impact on the pumping power (pressure drop). The influence of amount of pores per inch on the total heat removal capacity of the heat sink material under consideration is almost insignificant except at the low Reynolds numbers for 40 PPI sample. This finding is consistent with the results of Tzeng and Jeng [13]. Total heat removal performance of sample C is better than the others when Reynolds number is nearly less than 4000. This is due to fact that heat transfer area increases with increasing amount of pores per inch and this leads to an enhancement on the convective heat transfer especially at the low values of Reynolds number.

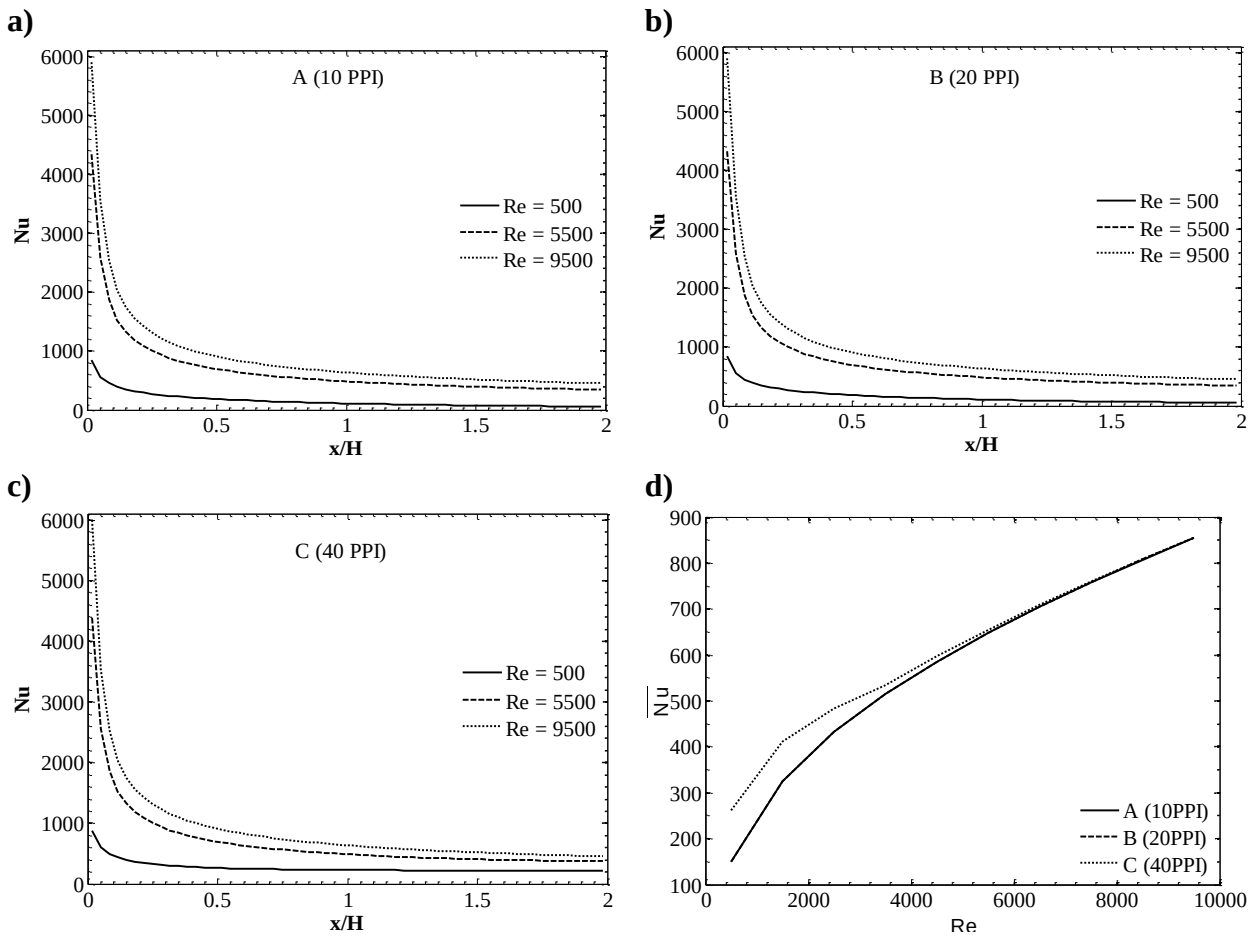

Figure 3. Variation of *Nu* and $\overline{Nu}$ with *Re* for 10, 20 and 40 PPI aluminum foams.

6. Summary remarks

The fluid flow and heat transfer characteristics of air cooled block type 10, 20 and 40 PPI aluminum foam heat sinks placed in a rectangular channel are studied numerically for various values of Reynolds number. Numerical results reveal that the plug flow condition inside the aluminum foam heat sinks of different pore densities is in existence. Increasing Reynolds number results in an increase in average Nusselt number and pressure drop along the flow direction. The

effect of pores of per inch on the average Nusselt number is negligibly small except for sample C when Reynolds number is less than 4000. However, the amount of pores per inch has a considerable influence on the pressure drop.

References

[1] Li H.Y., Leong K.C., Jin L.W., Chai J.C. Analysis of fluid flow and heat transfer in a channel with staggered porous blocks. International Journal of Thermal Sciences 2010:49:950-962.

[2] Solmuş İ. Numerical investigation of heat transfer and fluid flow behaviors of block type graphite foam heat sink inserted in a rectangular channel. Applied Thermal Engineering 2015:78: 605-615.

[3] Yang Y.T., Hwang M.Lu. Numerical simulation of turbulent fluid flow and heat transfer characteristics in heat exchangers fitted with porous media. International Journal of Heat and Mass Transfer 2009:52:2956-2965.

[4] Dukhan N., Chen K. Heat transfer measurements in metal foam subjected to constant heat flux. Experimental Thermal and Fluid Science 2007:32:624-631.

[5] Leong K.C., Jin L.W. Effect of oscillatory frequency on heat transfer in metal foam heat sinks of various pore densities. International Journal of Heat and Mass Transfer 2006:49: 671–681.

[6] Feng S.S., Kuang J.J., Wen T., Lu T.J., Ichimiya K. An experimental and numerical study of finned metal foam heat sinks under impinging air jet cooling. International Journal of Heat and Mass Transfer 2014:77:1063–1074.

[7] Hunt M. L., Tien C. L. Effects of thermal dispersion on forced convection in fibrous media. International Journal of Heat and Mass Transfer 1988:31:301–309.

[8] Calmidi V.V., Mahajan R.L. The effective thermal conductivity of high porosity fibrous metal foams. ASME Journal of Heat Transfer 1999:121:466–471.

[9] Calmidi V.V., Mahajan R.L. Forced convection in high porosity metal foams. ASME Journal of Heat Transfer 2000:122:557-565.

[10] Jeng T.M., Tzeng S.C. Numerical study of confined slot jet impinging on porous metallic foam heat sink. International Journal of Heat and Mass 2005:48:4685-4694.

[11] Patankar S.V. Numerical Heat Transfer and Fluid Flow. McGraw Hill-Hemisphere, New York, 1980.

[12] Yang Y.T., Hwang M.L. Numerical simulation of turbulent fluid flow and heat transfer characteristics in heat exchangers fitted with porous media. International Journal of Heat and Mass Transfer 2009:52:2956-2965.

[13] Tzeng S.C., Jeng T.M. Convective heat transfer in porous channels with 90-deg turned flow. International Journal of Heat and Mass Transfer 2006:49:1452-146.